Evolutions of Vortex Flow Control Design at High Flow Rates

I2 Report

Benjamin Engel
Candidate No. 0170976

Department of Engineering
University of Exeter

June 20, 2011

Abstract

In this investigation, a Vortex Flow Control (VFC), more specifically a Hydro-Brake® designed by Hydro-International, is modelled and tested computationally. A VFC is generally used to control the release of storm water back into the environment. Previous work has shown that a VFC is highly effective at preventing flooding and pipe damage. Single-phase, steady state solvers were used to model the initial VFC with a circular outlet, with the model being optimised numerically to ensure an accurate solution. Following this, modifications to the outlet geometry were made. It was replaced with both a square and a triangular shaped outlet to test for the effect this had on the performance of a VFC. The computational model successfully predicted the formation of a vortex and core, with backflow being shown. Results were validated against experiments carried out by Worrall (2011), with an average difference of less than 10% between the two being found. It was concluded that the efficiency of a VFC is highly dependent on the maximum possible vortex size in the outlet. The circular outlet, having the largest vortex size, produced the most efficient head at high flow rates, followed closely by the square then the triangle.

Keywords: Vortex Flow Control, VFC, turbulence, single-phase, urban drainage

Acknowledgements

I would like to thank Gavin Tabor for his excellent supervision throughout the project. His guidance and advice made all the difference between a successful and a failed project. Secondly I would like to express my gratitude to Daniel Jarman from Hydro-International, whose tips and experience in the field have been a lifesaver when things looked hopeless. Finally, I would like to thank the rest of the Group Project team, especially Gautier Queguineur and Nicholas Williams for their input and company.

Contents

List of Figures

1 Introduction

As a result of the ever increasing population in urban areas, effective and reliable drainage systems are an incredibly important factor in ensuring the safety and hygiene of inhabitants. The floods of 2007 and more recently, earlier this year, have resulted in the topic of climate change being brought to the forefront of government attention. One result of this is the Flood and Water Management Bill, providing, amongst others more thorough management of flood risk. A large aspect of this flood management is the implementation of Sustainable Urban Drainage Systems (SUDS) in all new urban developments. SUDS are designed to reduce the impacts of new or existing urban developments on surface drainage by attempting to mimic or improve the surface drainage as it was before development. Rather than attempting to achieve the huge storage capacity that would be required for stormwater runoff, SUDS are designed to regulate and slow the release of water back into the environment. These devices include, amongst others, the Hydro-Brake® (henceforth referred to as hydro brake, or VFC) flow control designed by Hydro International Plc. (`http://www.hydro-international.biz/`) one of the UK's leading manufacturers of sustainable drainage systems. Over 60% of the floods in 2007 were as a direct result of the drainage infrastructure's inability of dealing with the large volumes of water, further emphasising the importance of optimally designed SUDS and their installation in all future urban developments.

2 Objectives

2.1 Group

The primary focus of this research project will be on the afore-mentioned Hydro-Brake Flow Control. This is a vortex flow control (VFC) unit that, as its name suggests, regulates the flow in an urban drainage system by employing the concept of vorticity. At low flow rates (equivalent to day-to-day rainfall) the VFC allows water to flow through with little to no head loss. At high flow rates, however, a vortex forms in the system, which effectively chokes the flow, resulting in high head loss and a lower flow rate.

The objective of the project will be to examine a variety of alternative shapes of the VFC, attempting to obtain a more efficient design. The primary focus is on modifying the size and shape of the outlet. Possible areas for further research depending on success will be size and shape of overall VFC and of the inlet.

The project will be divided into three main sections, namely computational modelling, experimental testing and urban drainage modelling:

- The computational team will use computational fluid dynamics (CFD) to investigate and attempt to model various vortex formation scenarios, including modelling of the experimental setup and various designs of the Hydro-Brake Flow Control. Various turbulence models and mathematical approaches will be employed through the use of the open source CFD software package OpenFOAM.
- The experimental team will develop a test rig in order to investigate the formation of vortices in practice. Various experimental measurements, including pressure, will be used to to validate the computational data provided by the CFD team. In addition, the experimental team will be testing various prototypes built by the Hydro laboratory facilities in Clevedon.
- The urban drainage team will be employing two different software types to simulate rainfall runoff in an urban drainage situation, namely InfoWorks CS (MWH Soft - `http://www.mwhsoft.com/products/infoworks_cs/`) and the Storm Water Management Model (U.S. Environmental Protection Agency - `http://www.epa.gov/ednnrmrl/models/swmm/`). Comparisons between the two pieces of software will be made through the simulation of various drainage systems with included VFCs.

2.2 Individual

TThe CFD has been further divided into three individual sections. The first will require close collaboration with the experimental team, modelling the test rig and its variations along with the laboratory setup from Hydro-International for result comparison. The second and third parts of the CFD will be modelling the VFC with multiple outlet shapes at various flow rates. One team member will be responsible for modelling the VFC at very low flow rates, before kickback occurs, when the VFC can still be considered an orifice plate. The second team member will be modelling the high flow rates, post kickback, where vortex flow is occurring.

The main aim of this individual report and following investigations will be the aforementioned 'third' section of the CFD areas. Mathematical optimization will be performed to ensure the best possible model accuracy and computational speed. Once data is as close to experimental data as possible, modifications will be made in conjunction with the experimental team, attempting to optimize and improve the current Hydro-Brake Flow Control.Three different geometries will be modelled at various post kickback flow rates in order to ascertain which outlet shape performs best. More specifically, the

computational models will have the same dimensions and characteristics as the experimental setup at Hydro-International. For this setup, kickback occurs at a flow rate of around $4.5L/s$, as seen in Fig. 13. Flush flow is the flow rate at which the vortex formation occurs, after which the fluid characteristics transition to kickback flow, where flow begins to attain the properties of a typical orifice plate.

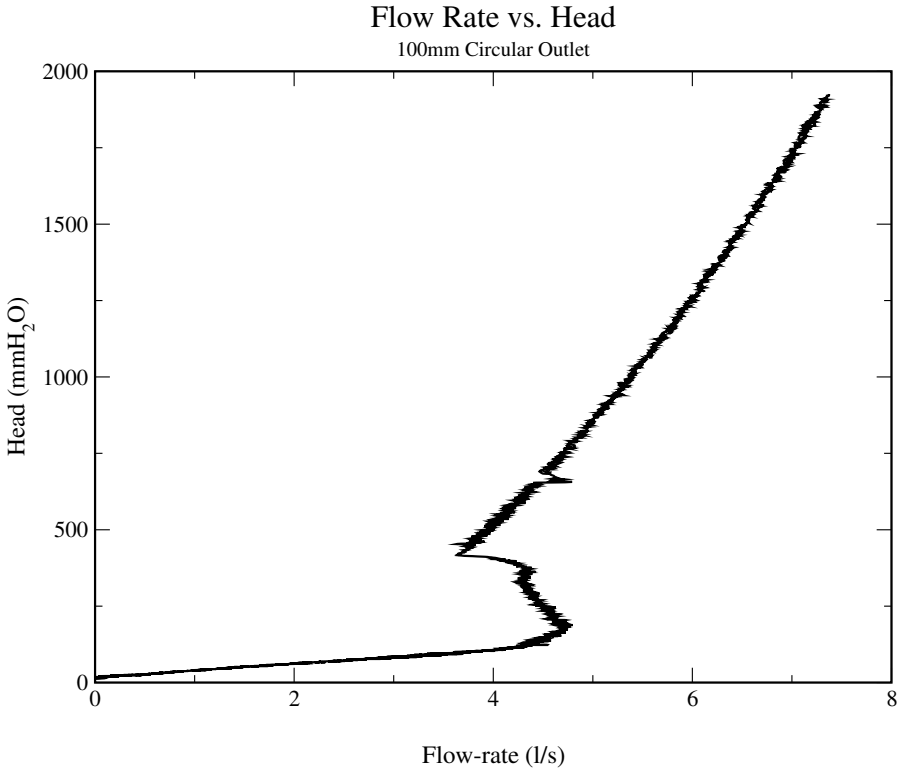

Figure 1. Demonstration of sample experimental results for a Hydro-Brake flow control, with kickback occurring at $5l/s$ for a VFC with a $100mm$ circular outlet (Hydro-International, 2010).

3 Vortex Diodes

Fluidic systems like the VFC - or vortex diode as it is more commonly known - are used throughout a wide range of engineering practices, ranging from the nuclear industry to urban drainage. A vortex diode contains no moving parts, making it relatively maintenance free (abrasion from particles can become an issue, especially in urban drainage) and cheap to produce. A vortex diode, as defined for this research project, consists of a round, disc-shaped chamber with one tangential inlet and one axial outlet, as seen in Fig. 2.

If flow entering the tangential port is below defined 'storm-water' criteria, i.e. if the flow rate is low, the diode acts like an orifice plate, with little to no pressure drop. At

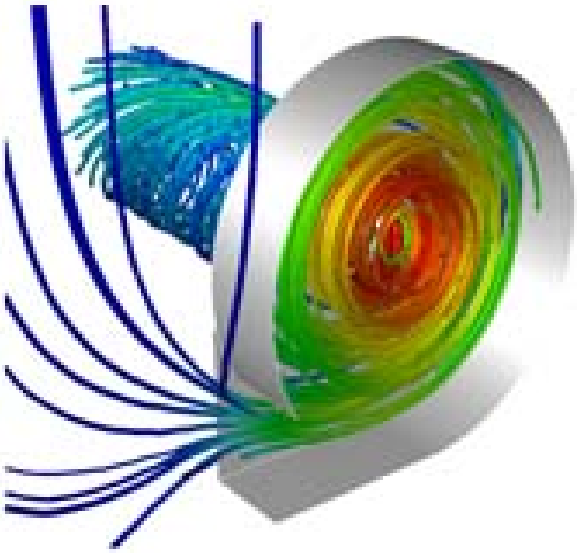

Figure 2. An example of a vortex diode or VFC as used for this research project (Jarman *et al.*, 2009).

high flow rates the flow sets up a vortex, establishing a large pressure drop across the device, these two phases are depicted in Fig. 3. This pressure drop effectively reduces the volume of discharge, staggering it, thereby preventing flooding.

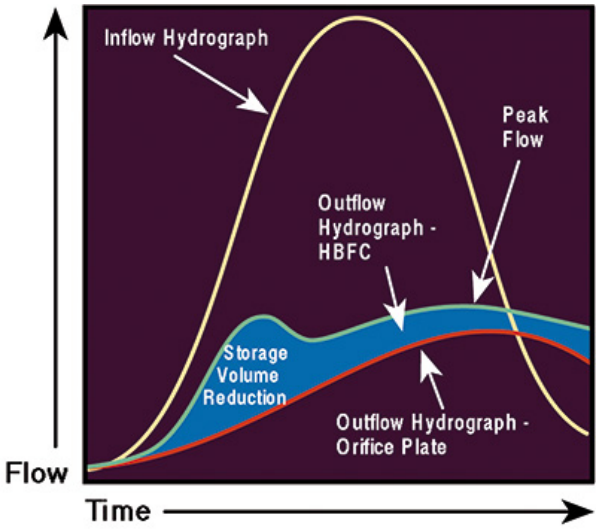

Figure 3. A hydrograph of a Hydro-Brake Flow Control (Hydro-International, 2010).

The performance of a vortex diode can be characterized in terms of its diodicity, or the ratio of the reverse flow (tangential to axial flow) pressure drop to the forward flow (axial to tangential flow) pressure drop for the same flow rate (Kulkarni *et al.*, 2009), i.e. $D = \frac{\Delta P_r}{\Delta P_f}$.

Efficient use of a VFC requires some form of storage system, generally in the form of a tank, to store excess fluid. The VFC chamber itself is characterized by the inlet/outlet diameters and its height, which decide the volumetric flow rate through the VFC and the point of transition to vortex controlled flow. Incorrect storage or VFC design can have adverse effects on drainage, causing flooding or damage, as a result, VFC design is crucial.

4 Current Literature

The concept of a vortex diode was first introduced by Zobel (1930). As a result of the high turbulence, the flow in a vortex diode is inherently transient. Jacobes (1972) confirmed the unsteadiness experimentally, his results showing the flow rate variation as depicted previously in Fig. 3.

Over the past few decades, multiple published literature pieces, including both experimental and theoretical work by, amongst others, Priestman & Tippetts (1984), and Priestman (1987) have shown that the tangential flow velocity (more commonly known as swirl) increases progressively towards the center of the diode. This velocity increase does not continue to the exact center of the diode, at a point of critical radius the tangential velocity becomes linearly proportional to the radius itself. As found by Kulkarni *et al.* (2008), the tangential flow can be divided into two distinct zones, constant circulation (free vortex region) and the forced vortex region. This point of transition is strongly dependent on the diode geometry, however the effect of these regions on diode optimization are as yet not thoroughly investigated. Attempts at testing this were made by Stairmand (1990) who used an analysis extended from that of Wormley & Richardson (1970), whereby an extended boundary layer coefficient (BLC*) represented the free to forced vortex transition based on the Reynolds number, chamber dimensions and a ratio of tangential to radial velocity. It was found that the forced vortex region increases as BLC* increases, up to a BLC* of 2 where the majority of the chamber is filled by it.

Confined swirling flow on a more general level has been investigated extensively and will also be reviewed in detail owing to its strong applicability to the VFC case.

Jakirlic *et al.* (2002) experimented computationally with several types of swirling flows with various Reynolds numbers and swirl intensities, attempting to identify specific features needing to be taken into account when modelling turbulence. Flow geometries analysed included, turbulent channel flows with streamwise/spanwise rotation or sta-

tionary/moving boundaries and swirl flows in combustor chambers and long tubes. The performances of multiple variations of the second-moment closure (Reynolds Stress Models - RSM), including both high and low Re versions, and of eddy-viscosity (e.g. k-ϵ and low Re variants) turbulence models were compared for each of the cases. It was found that second-moment models were significantly superior, especially at wall boundaries. These models agreed the most with experimental data and direct numerical simulations (DNS). Despite this, results for the normal stress components in the core region were inaccurate. It was found that the differences between upwind (first order) differencing and central (second order) differencing were minimal.

To further investigate the potential of second-moment closure models, Jawarneh & Vatistas (2006) examined vortex chamber flows with high swirl numbers. Reasonable agreement was found between experimental and computational data, with free to forced vortex transition and reverse flow accurately predicted and the pressure drop predicted to within $\pm 10\%$. The swirl number was found to have a distinct impact on the flow characteristics, with the vortex core decreasing in size along with the swirl number. This resulted in greater pressure drops and higher tangential velocities.

Expanding upon the Reynolds Averaged Navier Stokes (RANS) solutions obtained by Jakirlic *et al.* (2002), Derksen (2005) performed Large-Eddy Simulations (LES) of the turbulent flow in a swirl tube with a tangential inlet and compared these to experimental data obtained from the same case through the use of laser Doppler anemometry (LDA).

The advantage of LES over RANS is a greater resolution of the small scale unsteadiness, allowing for calculation of turbulence much smaller than would be possible with RANS as well as more accurate results for particle transport. Secondly, swirling flows often display almost periodic fluctuations (Derksen & Van den Akker, 2000) that cannot be distinguished from turbulence fluctuations. This makes LES a preferable choice as there is an absence of a spectral gap between them. Computational simulations confirmed that the flow field is highly dependent on the outlet diameter, very high velocity gradients were encountered for the narrowest pipe diameter. The tangential velocity was found to more than linearly increase with the ratio of swirl tube to exit pipe diameter.

More recently, Yin *et al.* (2010) used LES to model unsteady flow in a vortex diode, where a very good agreement was found with experimental data, as seen in Fig. 4. The appropriateness of LES for simulating flow through vortex diodes was confirmed.

The multitude of literature over the past decades has shown that although the most accurate method of modelling swirl is LES, second-moment closure and eddy viscosity models can provide relatively similar results , although the predictions for tangential velocity profiles and boundary layer results are less accurate.

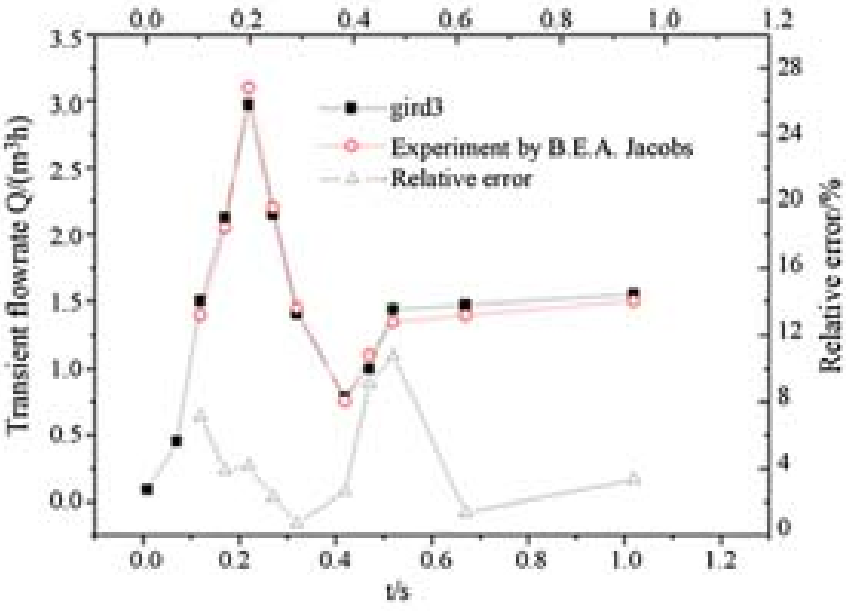

Figure 4. Comparison between experimental data and LES results (Yin *et al.*, 2010)

5 Mathematical Background

The following governing equations are used to describe the transport of mass, momentum and energy through a fluid. The differential form of the mass conservation equation for an incompressible fluid is:

$$\frac{\partial u_i}{\partial x_i} = 0 \tag{1}$$

The differential form of the Navier-Stokes equation (for incompressible Newtonian fluids) is:

$$\frac{\partial(\rho u_i)}{\partial t} + \frac{\partial(\rho u_i u_j)}{\partial x_j} = \mathbf{F}_i - \frac{\partial p}{\partial x_i} + \frac{\partial}{\partial x_j} + \left[\mu\left(\frac{\partial u_i}{\partial x_j} + \frac{\partial u_j}{\partial x_i}\right)\right] \tag{2}$$

Where $\mathbf{F}_i$ is the body forces and *i, j, k* represent a three dimensional domain. The differential form of the energy conservation equation, once again without a viscous dissipation term is:

$$\frac{\partial(\rho c_p T)}{\partial t} + \frac{\partial(\rho c_p u_i T)}{\partial x_j} = \frac{\partial}{\partial x_j}\left(\Gamma_e \frac{\partial(c_p T)}{\partial x_j}\right) + S_T \tag{3}$$

Where Γ_e is the appropriate molecular diffusivity and S_T is the rate of creation of the property per unit volume.

6 Turbulence

Turbulence is a fluid state attributed by chaotic, seemingly random property changes. Included in this are rapid pressure and velocity changes, low diffusion and high convection. Although there is no direct, proven relation between turbulence and the Reynolds number, it is often the case that a high Re will result in a turbulent flow. In the case of this research project it is predicted that values will range from 23000 to 1000000.

Turbulence results in the formation of eddies, all of different length scales. The majority of turbulent kinetic energy is contained within the large scale eddies, which then "cascades" (Mathieu & Scott, 2000) to the smaller scale structures. This process continues, with smaller structures continuously being created and a hierarchical structure of energy cascading eddies is formed. Eventually, these eddies reach such minuscule sizes as to affect molecular diffusion, and viscous dissipation of energy occurs. Solving for the turbulence aspects of a problem is possible using the NS equations, however at very large Re these solutions tend to be unstable. Due to flow variables such as velocity and pressure being dependent on time, a statistical description is needed to increase the probability of stability.

6.1 Numerical Characterization

The Russian mathematician Andrey Kolmogorov proposed the first statistical theory of turbulence (Benzi & Frisch, 2010), which decomposes a turbulent quantity, Ψ, into two aspects, a time averaged and a fluctuating part:

$$\Psi(\mathbf{x}, t) = \bar{\Psi}(\mathbf{x}) + \Psi'(\mathbf{x}, t) \tag{4}$$

Where $\mathbf{x} = (x, y, z)$ is a three dimensional position vector.
For a flow that decays in time, Reynolds averaging can be applied to the Navier Stokes equation (RANS 2), resulting in a statistical stationary flow with no time dependent terms remaining:

$$\rho \frac{\partial u_j u_i}{\partial x_j} = \rho \bar{\mathbf{F}}_i + \frac{\partial}{\partial x_j} \left[-\bar{p}\delta_{ij} + 2\nu \bar{S}_{ij} - \rho \overline{u_i' u_j'} \right] \tag{5}$$

Where $\bar{S}_{ij} = \frac{1}{2} \left(\frac{\partial \bar{u}_i}{\partial x_j} + \frac{\partial \bar{u}_j}{\partial x_j} \right)$ is the mean rate of strain tensor and $-\rho \overline{u_i' u_j'}$ is referred to as the Reynolds Stresses term.

6.2 Applicable Turbulence Models

In order to fully solve the Navier Stokes equations, additional data is required, namely the Reynolds stresses. To do so, further transport equations need to be solved. This

is done through the use of turbulence models including, for example, standard k-ε and SST. Owing to the large variety of turbulence models that will be used in this project, they will merely be briefly introduced according to their mathematical base. For more detailed breakdowns of each model, refer to, amongst a huge variety of sources available, `http://www.cfd-online.com/Wiki/Turbulence_modeling`.

6.2.1 Linear Eddy-Viscosity Models

Reynolds stresses that are obtained from RANS equations are modelled by a linear relationship with the mean flow straining field, also known as the Boussinesq hypothesis.

$$-\rho < u_i u_j >= 2\mu_t S_{ij} - \frac{2}{3}\rho k \delta_{ij} \tag{6}$$

Where μ_t is the eddy viscosity, k the mean turbulent kinetic energy and S_{ij} the mean strain rate.

In their most popular form, these are two equation models, containing two extra transport equations to represent the turbulent flow characteristics. In most cases this includes the turbulent kinetic energy, $k = \frac{3}{2}vI$ (where $l \approx 0.07D_H$ and $I \approx 0.16Re^{-\frac{1}{8}}$) and, most popularly, either the turbulent dissipation, $\epsilon = C_\mu^{\frac{3}{4}} \frac{k^{\frac{3}{2}}}{l}$, or the specific dissipation, $\omega = C_\mu^{-\frac{1}{4}} \frac{\sqrt{k}}{l}$. These are referred to as the standard $k-\epsilon$ (Launder & Sharma, 1974) and $k-\omega$ (Wilcox, 1988) models respectively. There are multiple variations of these models which can be found discussed in detail in, amongst others, the paper by Uddin (2008).

6.2.2 Second-Moment Closure Models

Often referred to as Reynolds Stress Models, these ignore the eddy viscosity approach and, instead, the Reynolds stresses, $\rho\overline{u_i' u_j'}$, are directly calculated. These stresses are then used for closure of the Reynolds-averaged momentum equation. Variations include the Speziale-Sarkar-Gatski (Speziale *et al.*, 1991) and Launder-Reece-Rodi (Launder *et al.*, 1975) models.

6.2.3 Large Eddy Simulation

Based on the idea that eddies considered large in relation to model geometry are influenced by it, whereas small eddies are universal. LES explicitly solves for the large eddies in a model and accounts for the small eddies with a subgrid-scale (SGS) model. The velocity field is mathematically divided into a resolved and a sub-grid part $\mathbf{v} = \bar{\mathbf{v}} + \bar{\mathbf{v}}'$

with a spatial filter G applied.

$$\bar{\mathbf{v}} = G \times \mathbf{v} = \int_D G(\zeta, \Delta)\mathbf{v}(\zeta, t)d^3\zeta \tag{7}$$

Where Δ is the filter width of G and D the computational domain. From this it can be implied that the filter width is equivalent to the cell size, explaining the labelling convention of GS and SGS. One of the more popular LES models is that devised by Smagorinsky (1963), which will be the one employed in this project as it is the one most often employed in previous literature, allowing for the best comparison. For more information on LES and the mathematical definitions, refer to Tabor & Baba-Ahmadi (2008).

7 Numerical Background

This chapter provides a brief introduction to the numerical methods used by OpenFOAM and this specific case.

7.1 Finite Volume Method

The finite volume method is a discretization scheme for flow domains. The flow domain is divided into a finite quantity of control volumes. The integral forms of the transport equations are numerically integrated for each control volume. This results in a series of partial differential equations (PDEs) to which specified discretization techniques are applied (explained in detail in Section 7.2. The final result is a finite number of linear equations, solvable using matrix techniques. Values at other locations in space are obtained by interpolation. Further mathematical detail can be found in, amongst others, the publication by Toro (1999). OpenFOAM uses a variety of specifiable schemes and solutions which are applied to the integration process at run time, affecting the mathematical order of accuracy, this is discussed in greater depth in Section 8.

The transport equations are integrated:

$$\int_V \frac{\partial(\rho\Psi)}{\partial t}\mathrm{d}V + \int_V \frac{\partial(u_i\rho\Psi)}{\partial x_i}\mathrm{d}V = \int_V \frac{\partial}{\partial x_i}\left(\Gamma_\Psi \frac{\partial\Psi}{\partial x_i}\right)\mathrm{d}V + \int_V S_\Psi \mathrm{d}V \tag{8}$$

Where Ψ represents an arbitrary scalar variable like velocity or pressure, Γ_Ψ represents the transport coefficient (e.g. turbulent viscosity) and S_Ψ the sum of all sources (including pressure gradient). The volume integrals in equation 8 are converted to surface

integrals through the use of the Gauss divergence theorem:

$$\overbrace{\int_V \frac{\partial(\rho\Psi)}{\partial t}\mathrm{d}V}^{\text{Time}} + \overbrace{\underbrace{\int_V \left(\rho u_i \Psi - \Gamma_\Psi \frac{\partial \Psi}{\partial x_i}\right) n_i \mathrm{d}\sigma}_{\text{Flux}} = \underbrace{\int_V S_\Psi \mathrm{d}V}_{\text{Source}}}^{\text{Space}} \tag{9}$$

Where σ is a surface enclosing a volume V and n_i is the projection of the unit vector normal to the surface. This equation must be solved for each control volume.

7.2 Spatial Discretization

Various mathematical schemes can be employed to discretize the spatial part of equation 9. Those applicable to this thesis are described in brief below, for a more detailed breakdown of other available schemes, refer to McLachlan (1998)

7.2.1 Upwind

An upwind differencing (UD) scheme attempts to discretize partial differential equations by using differencing biased in the direction of characteristic flux although differentiation direction will always be upstream.

$$\phi_f = \begin{cases} \phi_f = \phi_P & \text{for} \quad F \geq 0 \\ \phi_f = \phi_N & \text{for} \quad F < 0 \end{cases} \tag{10}$$

Where F represents the mass flux through the face:

$$F \quad = \quad \mathbf{S}(\rho \mathbf{U}) \tag{11}$$

Where $\mathbf{S}$ is the outward pointing vector normal to the face.

Although this scheme prevents oscillations due to external factors, greatly increasing stability, it is only of first order accuracy in time and space. As a result of this, it is may not be sufficient for such a complex case as jet impingement. For large gradients (turbulence for example) this scheme introduces strong numerical diffusion, decreasing accuracy even further. Although second order upwinding schemes are possible, they are not easily employed in OpenFOAM so will not be discussed further.

7.2.2 Linear

Based on central differencing (CD) techniques, linear schemes are a second order approach for determining the flux through a face. The face value is calculated according

to:

$$\phi_f = f_x\phi_P + (1 - f_x)\phi_N. \tag{12}$$

Where f_x is the interpolation factor defined as a ratio of distances between control volumes, $\overline{\text{fN}}$ and $\overline{\text{PN}}$ as shown in Fig. 5.

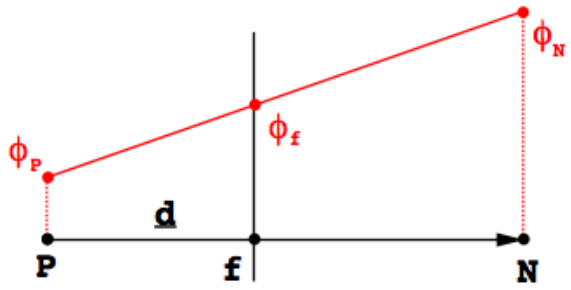

Figure 5. A demonstration of central differencing (Jasak (1996)).

7.2.3 limitedLinear

This scheme uses a blended differencing (BD) technique (Peric (1985)), it is a combination of CD (Eqn. 12) and UD (Eqn. 10).

$$\phi_f = (1 - \gamma)(\phi_f)_{UD} + \gamma(\phi_f)_{CD} \tag{13}$$

Where γ, $0 \leq \gamma \leq 1$, represents the blending factor which determines how much numerical diffusion (as a result of UD) will be introduced, with 0 being full UD.

7.3 Temporal Discretization

7.3.1 Euler

This is an implicit, first order scheme to solve initial value problems. It is numerically stable and often used to initialize higher order calculations that would otherwise be unstable. Applying it to a basic initial value problem:

$$\frac{\partial u}{\partial t} = f(t, u) \tag{14}$$

The scheme becomes:

$$u_{i+1} = u_i + nf(t_{i+1}, u_{i+1}). \tag{15}$$

Calculating $f(t_{i+1}, u_{i+1})$, based on a step size n, a set of equations have to be solved for each step. As a result, the accuracy is dependent on n.

7.3.2 Crank-Nicholson

A second order, implicit scheme it is unconditionally stable and based on central differencing:

$$u_i^{n+\frac{1}{2}} = \frac{1}{2}\left(u_i^{n+1} + u_i^n\right) \tag{16}$$

The stability of this scheme is greatly affected by the step size. This can be best represented by employing the Courant-Friedrichs-Lewy (CFL) condition. This is a necessary condition when explicit time stepping schemes are used for solving hyperbolic PDEs numerically. To prevent hugely inaccurate results, the timestep must be less than a CFL of 0.5, as shown in equation 17:

$$\text{CFL} = u\frac{\Delta t}{\Delta x} > 0.5 \tag{17}$$

As can be seen, this can also be affected by grid size, which is a logical assumption. This can be demonstrated with a simple wave propagation example. The smaller the grid, the smaller the time required for a wave to propagate through each grid point, resulting in a smaller required time-step in order to accurately calculate for the propagation.

To reduce computational time and power requirements, the Crank-Nicholson (CN) scheme can be blended with the implicit Euler scheme with a mixing coefficient of $0 < \psi < 1$ with 1 being fully CN and 0 fully Euler.

7.4 Reynolds Number

The Reynolds number is a ratio between inertial and viscous forces in a fluid, a factor which determines whether a flow is turbulent or laminar. It is represented by:

$$Re = \frac{\rho v L}{\mu} \tag{18}$$

where μ is the dynamic viscosity, v the velocity and L the characteristic length of the flow. For the case of a VFC the choice of what measurement to use for L varies in previous work. Primarily it is taken as the inlet or outlet diameter/length. For this report the inlet was rectangular, so the side length was used. As a result, 18 is modified to account for this, where L is replaced by the hydraulic-diameter, $D_H = \frac{4A}{P}$, where P is the wetted perimeter and A the cross-sectional area of the inlet.

7.5 Hydraulic Head

Head is a term that relates the energy in an incompressible fluid to the equivalent height of a static column of the same fluid. It is expressed in units of height (m) and can be derived from the Bernoulli Equation.

$$H = \frac{v^2}{2g} + \frac{P}{\rho g} \tag{19}$$

where H is the total head, $\frac{v^2}{2g}$ the velocity head and $\frac{P}{\rho g}$ the pressure head. P being the gauge pressure, ρ the density, g the acceleration due to gravity and v the fluid velocity.

8 OpenFOAM

OpenFOAM is primarily a C++ based CFD library used to create and run two types of executable, solvers and utilities. Solvers are designed to solve specific case types in continuum mechanics, including combustion, buoyant flow, electromagnetic and stress distributional problems. Utilities provide data manipulation and visualisation functionality, including sample, Paraview and blockMesh. The OpenFOAM structure is depicted in Figure 6.

OpenFOAM is accompanied by a user manual (Documentation (2011)), which provides introductory descriptions on operation of OpenFOAM, various tutorials and detailed breakdown of OpenFOAM individual components if further reference is required.

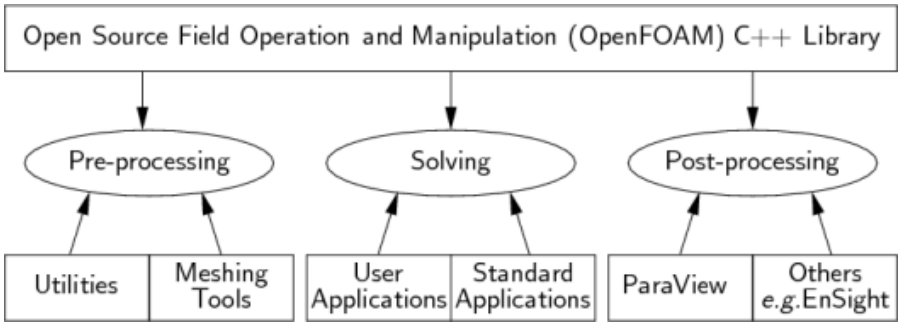

Figure 6. A basic breakdown of OpenFOAM

To date, the most recent release is 1.7.x (released 26/06/2010) which was employed for the duration of this thesis.

8.1 Case Structure

An OpenFOAM case consists of multiple modules where all aspects are configurable. The base directory structure for minimal required functionality is shown in Figure 7 (Documentation (2011) Ch. 4.1).

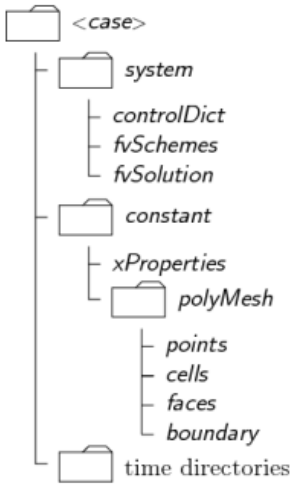

Figure 7. The OpenFOAM case structure.

These requirements include:

- constant - This directory contains a full description of the case mesh in a sub directory (polyMesh) and the physical properties required for the case (e.g. thermophysicalProperties & transportProperties).
- system - Mathematical schemes and parameters are located in this directory. This includes controlDict for setting run time and time steps, fvSchemes where discretisation schemes for variables can be set and fvSolution where equation solvers, tolerances and mesh correctors can be set. For parallel cases like this thesis, the decomposeParDict file is used to specify case and grid decomposition parameters for each processor.
- Time directories - These include the 0 folder, where boundary conditions and initial values are defined by the user and further time directories that are written by OpenFOAM as the simulation progresses (at time intervals definable in controlDict)

Meshes can either be imported via utilities like fluent3DToFoam or created in OpenFOAM via blockMesh, a utility that generates meshes based on a user defined description in a dictionary style file (blockMeshDict).

For post processing, results can either be directly imported into a plotting application like Tecplot, or they can be further visualised in OpenFOAM's third party visualisation software, Paraview, using a utility named paraFoam.

8.2 Patches and Boundary Conditions

Meshes are broken up into multiple patches, each with various definition possibilities in the boundary file of the constant/system directory. The type is patch for all except those that have some form of geometrical constraint applied (e.g. symmetry: symmetryPlane) and empty patches. For this report, the following were employed:

- patch - The generic patch type, it needs to be further defined by boundary conditions (BCs).
- empty - Front and back planes of a 2D geometry
- symmetryPlane - Plane of symmetry
- wall - Used for wall functions in turbulent flows

As a result of all schemes and solutions being user-specified, OpenFOAM is very sensitive to correct boundary conditions (BC). Boundary conditions can be divided into three types, base (describes patch in terms of geometry), primitive (numerical condition assigned to a field variable) and derived (complex condition, derived from the primitive type). For a list of all available BCs, the user should refer to the OpenFOAM source code. A few examples are listed below:

- symmetryPlane (*base*) - used to decrease computational requirements of a case by dividing it along lines of symmetry and specifying a flux gradient of 0.
- fixedValue (*primitive*) - variable is specified, i.e. fixed for that patch, for example velocity at nozzle outlet or for specifying no-slip conditions at walls.
- zeroGradient (*primitive*) - normal gradient of variable is zero, used for turblence variables at walls or to define adiabatic conditions.
- calculated (*primitive*) - value is calculated by OpenFOAM, i.e. obtained by numerical analysis.
- inletOutlet / outletInlet (*derived*) - These conditions allow for backflow at inlet / outlet respectively. They switch between zeroGradient and fixedValue depending on flow direction (inletOutlet: incoming fluid = fixedValue & outgoing fluid = zeroGradient, vice versa for outletInlet).

- pressureInletOutletVelocity (*derived*) - a modification of the inletOutlet BC, velocity is calculated from the flux normal to the patch if the pressure is known. This makes backflow dependent on the pressure distribution rather than a fixed value.
- kqRWallFunction / epsilonWallFunction / nutWallFunction (*wall function*) - a special BC for walls, more accurate than a zeroGradient condition. A mathematical function is applied to the wall in question to solve for fields at the boundary. A variety of functions are available and can be found in the OpenFOAM installation directory under turbulenceModels.

8.3 Numerical Schemes and Solutions

Found in the CASEROOT/system directory, the fvSchemes and fvSolution files dictate, amongst others, what numerical schemes, solvers, tolerances, smoothers and relaxation factors to apply to each field variable. The schemes used for the time, div, laplacian and grad terms have already been described in Section 7.

The fvSolution file allows the user to apply specific solvers to each field variable, (for example, icoFoam solves for velocity and pressure, so the user would need to specify the desired solvers for each variable). There are multiple types available, each varying in computational requirements, accuracy and stability. Each solver has a required set of parameters, including tolerance, relTol and preconditioner. OpenFOAM will inform the user if incorrect solvers or parameters are used (e.g. a symmetric matrix solver applied to an unsymmetric matrix).

Solver tolerance ensures that residuals stay below desired levels with reduced tolerance resulting in exponential computational time requirements. A further sub-dictionary is relaxationFactors which controls under-relaxation, a technique that improves solution stability. Under-relaxation is specified by a factor, α, $0 < \alpha < 1$, with 1 being no relaxation and 0 representing a solution that does not change at all. It limits the amount a variable changes between iterations, ideal for steady-state simulations, dangerous for transient solutions where large change between iterations is expected, if not desired. There are many more specifiable parameters, some of which can be found in Ch. 5 of the Documentation (2011) and in the source code.

OpenFOAM employs either of two algorithms for the majority of it's solvers, the pressure-implicit split-operator (PISO) or the semi-implicit method for pressure-linked equations (SIMPLE). These are the iterative algorithms used to solve equations for pressure and velocity, PISO being employed for transient cases and SIMPLE for steady-state. Both algorithms are based on evaluating an initial solution and then correcting it, SIMPLE only makes 1 correction whereas for PISO it is specifiable (normally > 1 & < 4), this must be specified in the PISO sub-dictionary through the nCorrectors keyword. It was

found that the more correctors used, the higher the solution stability, although computational time increased drastically.

The modular approach of OpenFOAM ensures that the user has the complete freedom to choose which schemes / solutions to use. This can be seen as a disadvantage to the inexperienced user as many scheme / linear-solver combinations can result in highly unstable or inaccurate solutions.

8.4 Solvers

The solver employed for all of analyses was the steady state, incompressible simpleFoam solver. Additional comparisons between multiphase and transient flow was also desired but was beyond the time scale of this thesis.

9 Case Configuration

This project aims to investigate the effect of modifying the outlet shape on the performance and efficiency of the VFC. Three shapes will primarily be investigated, namely the original circular outlet as designed and implemented by Hydro International, and then both a triangular and a square shaped outlet, with various orientations (see Appendix A for details of the engineering designs for these geometries).

9.1 Domain

The basic domain for each case can be seen in Fig. 8, with only the outlet shape being modified on a case to case basis. The VFC itself has a square inlet of $100mm \times 100mm$, with the outlets maintaining a constant area across the geometries. The control (circular outlet) had a $100mm$ diameter, resulting in a side length of $135mm$ and $89mm$ for the triangular and square outlets respectively. A storage tank is used in all simulations for two reasons, it replicates the experimental setup used by Hydro-International and it was found that it significantly increased computational stability as well as eased boundary condition setup.

9.2 Mesh

Due to the complex flow fields involved in the computations and the interest in accurately resolving the vortex formation and core, very fine mesh resolution was required for the area inside the flow control. The mesh was created using Gambit (`http://www.ansys.com/`). It was significantly coarser in the tank itself as seen in Fig. 9. The mesh used contained 1 million cells, with a mesh refinement study confirming this as the desired resolution (See Section 9.3).

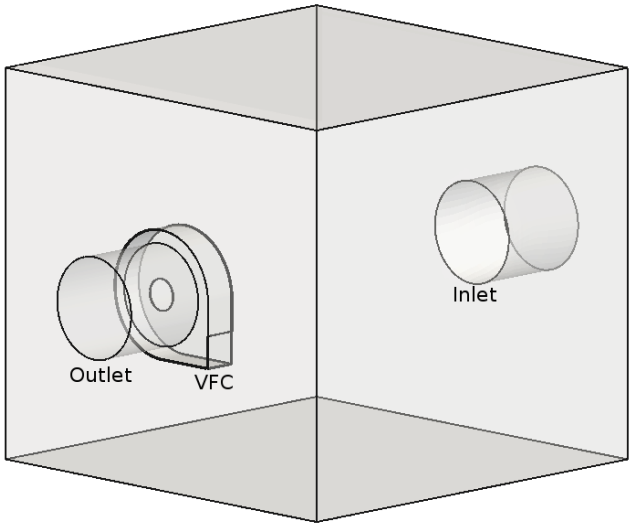

Figure 8. The computational domain for all cases, image obtained from Jarman (2011).

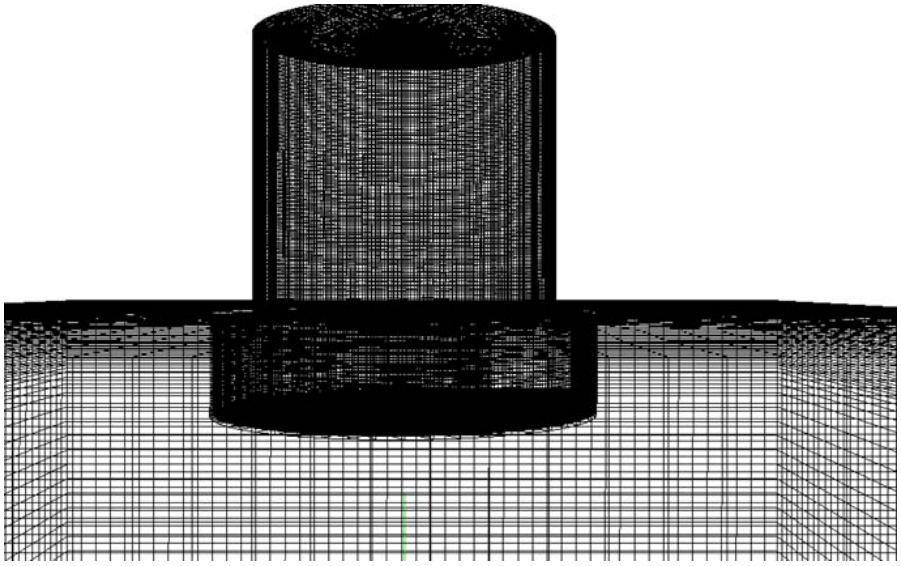

Figure 9. Part of the computational mesh, depicting the levels of resolution, with the highest being at and around the VFC itself.

9.3 Mesh Refinement

A control case with a circular outlet and constant flow rate of $6l/s$ was used as the basis for performing a mesh refinement study. The mesh resolution was modified until there was little to no change in the simulation results. An ideal number of cells was found to be around 1 million, as seen in Fig. 10.

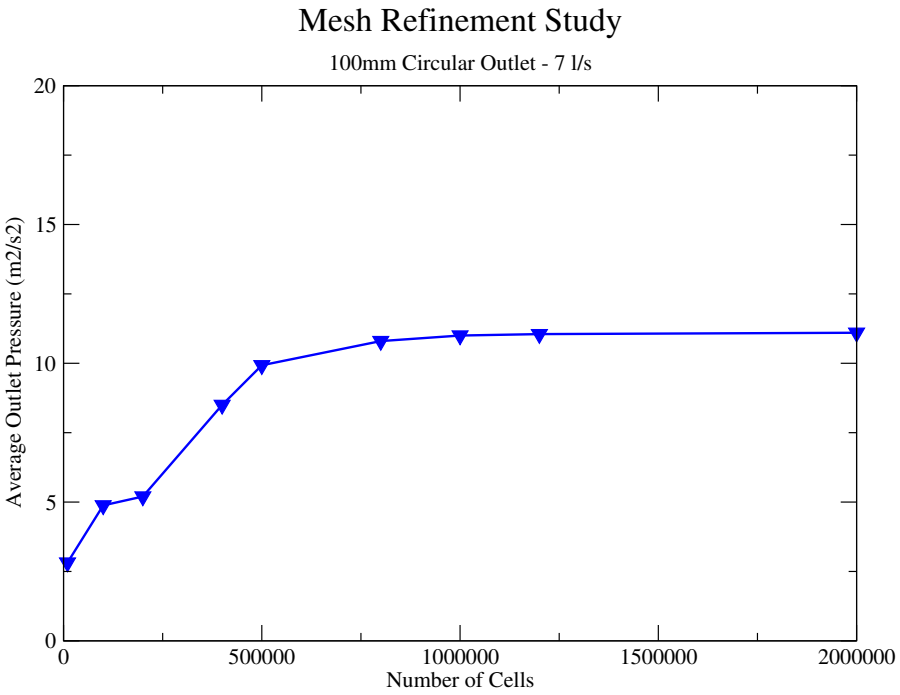

Figure 10. Mesh refinement study, comparing change in average outlet pressure to number of cells in the mesh.

9.4 Fluid Properties

The fluid was assigned the attributes of water at a temperature of 300K. This could be considered an inaccurate assumption, as fluid in a system will generally be affected by external temperatures which vary significantly over the course of the year in the UK. Further work would be required to determine the effect of modifying fluid temperature and its respective properties. Fluid between 293K and 303K from the tables arranged by Rogers & Mayhew (1995) was interpolated for a fluid at 300K. Fluid properties used are summarised below in Table 1

Dynamic viscosity	$\mu = 1.307 \cdot 10^{-3}\, Nsm^{-2}$
Kinematic viscosity	$\nu = 1.307 \cdot 10^{-6}\, m^2 s^{-1}$

Table 1. Fluid properties for the computational cases.

9.5 Boundary Conditions

Multiple flow velocities were used for each case in order to replicate the experimental data obtained as closely as possible. According to experimental data, kickback occurs in a VFC at a flow rate of 5 l/s, which implies a flow velocity of 0.5 m/s for the

default circular outlet case. To initialise the flow as turbulent, a turbulent intensity ($I = 0.16Re^{-\frac{1}{8}}$) of 0.045 was defined. From this, it was possible to obtain inlet values for k and ε using equations 20 and 21 respectively.

$$k = \frac{3}{2}(VI)^2 \tag{20}$$

$$\varepsilon = C_{\mu}^{\frac{3}{4}} \frac{k^{\frac{3}{2}}}{l} \tag{21}$$

Where V is inlet velocity and l is turbulent length scale, which can be approximated to $l \approx 0.07D$. Boundary conditions applied to each patch for each variable are listed in Tab. 2.

	TankWalls	**VFC**	**Inlet**	**Outlet**
p	zeroGradient	zeroGradient	zeroGradient	fixedValue
U	fixedValue	fixedValue	fixedValue	pressureInletOutletVelocity
k	kqRWallFunction	kqRWallFunction	fixedValue	zeroGradient
ε	epsilonWallFunction	epsilonWallFunction	fixedValue	zeroGradient

Table 2. Boundary conditions for the computational cases

Additionally, conditions used to initialize the Reynolds Stress models (k and ε) along with Reynolds numbers and inlet velocities are listed in Tab. 3.

$U(ms^{-1}$	Re	ε	k
0.5	38255.54705	0.000422163	0.000686432
0.55	42081.10176	0.000542171	0.000811026
0.6	45906.65647	0.000681288	0.000944419
0.7	53557.76588	0.001021096	0.001236863

Table 3. Values used for case initialization

9.6 Convergence and Tolerance Criteria

Optimal results were attained for a blended case that was partially 1st and 2nd order. All cases were run as steady state solutions in time. Divergence terms were run second order for all but the k and ε terms with respect to flux, with were run as first order upwind. Laplacian terms were blended using linearLimited with a blend factor of 0.3 (where 0 is fully first order and 1 is second).

For the primary case, a convergence tolerance of 10^{-6} was defined, with the relative tolerance (difference between iterations) being set to zero. A relaxation factor of 0.7 was

applied to the all but the pressure variable which had a lower relaxation factor of 0.3.

10 Results and Discussion

A total of 12 simulations were run, 3 geometries - triangle, square, and circular - with 4 flow rates (5, 5.5, 6 & 7 Ls^{-1}) each. All simulations were run until all residuals converged to at least $1e-5$. Every computation was initialized with a $k-\varepsilon$ turbulence model for 1000 iterations, after which they were all switched to a Launder Gibson Reynolds Stress Model and run to convergence - generally requiring around 25000-30000 iterations.

To ensure a homogeneous comparison between each geometry, total head loss in the system was calculated, which also allowed for comparison with experimental results (detailed in Section 7.5), this can be seen in Fig. 11.

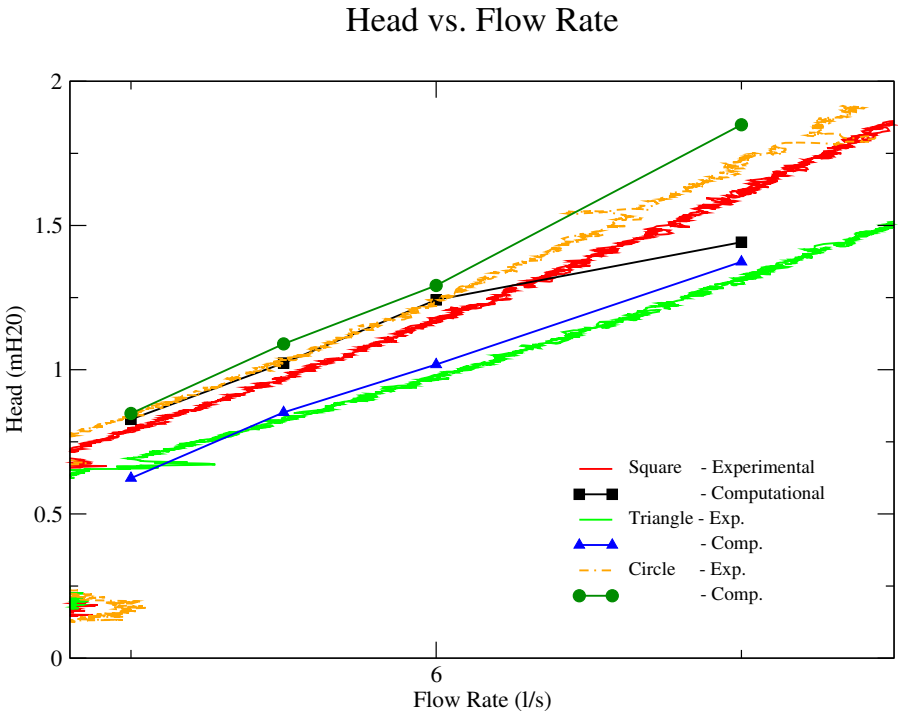

Figure 11. Total head comparison between experimental and computational results for various geometries at different flow rates. For origin of experimental data, refer to Worrall (2011)

There is a clear similarity between the experimental and computational data. For the simulated flow rates the values for head generally agree excellently. The head increase with flow rate is well predicted for all geometries. The greatest discrepancies seem to be at flow rates of $Q \geq 6.5Ls^{-1}$, where the computational results are either over or

under-predicted for the square and circular geometries. The difference (as a percentage magnitude) is depicted in Fig. 12.

Multiple attempts at modelling the kickback region and flow rates near it were made although obtaining a stable case was not possible with the computational and temporal resources available. It is therefore unexpected that the most similar results are closest to the kickback region of the VFC. The most likely suggestion for this is that as the flow rate increases, so does the degree of turbulence in the flow. The higher the turbulence, the greater the possibility for error in the solution due to the averaging performed by the RANS approach.

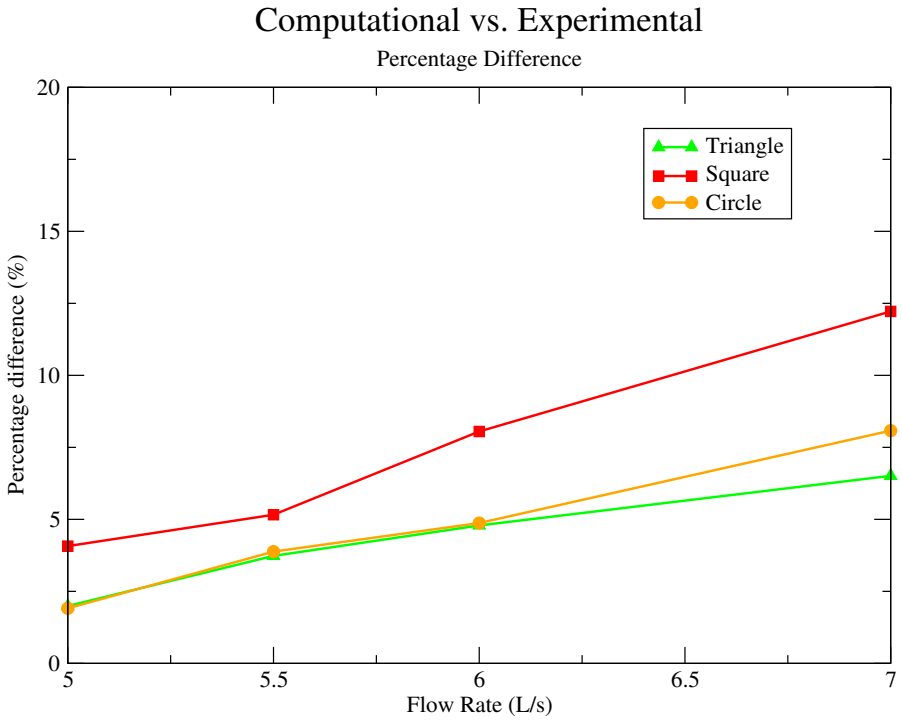

Figure 12. Percentage difference between experimental and computational results.

Although the RSTM turbulence model used is well known to be the most accurate for VFC modelling (see e.g. Kulkarni *et al.* (2008)), it was found that it is significantly more sensitive to boundary conditions than the two-equation variants. Initializing a case eases stability, however it was found that using anything less than 1000 time steps for initialization resulted in a non converging, incorrect case. Significant back flow was present in all cases for the first 800 time steps, as seen in Fig. 13. This is as a realistic result of the fluid flow rather than of incorrect case setup. Varying boundary conditions between the basic zeroGradient and its derived counter part inletOutlet which accounts for backflow made little difference. This behaviour is, however, expected in such a flow until it sufficiently develops and was first discovered by Jacobes (1972).

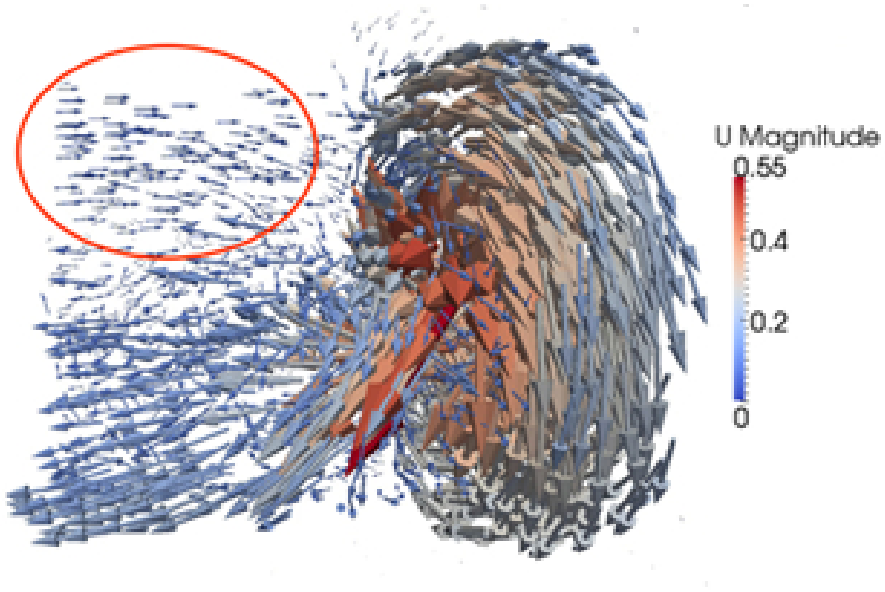

Figure 13. Pre 1000 iterations, showing initial backflow

Fig. 13 also shows the flow when developed, where backflow is no longer visible. It is here that the timestep data was used for initialization. In OpenFOAM, one does this by running the R utility on the initialization time step, which calculates the Reynolds Stresses for every cell at the specified time step.

Once all cases were run to convergence, Paraview 3.10, the foamCalc and the sample utility in OpenFOAM were used to post-process the data. sample makes use of a dictionary to read in user specified points, patches or lines in a mesh and samples them for defined variables at each time step. foamCalc can be used to calculate components of a vector type variable (e.g. velocity) or variable magnitude. Two lines through the VFC were extracted, one passing through the outlet and vortex core, another axially through the VFC. The velocity magnitudes and vertical (Uz) components were then calculated from the data. This allowed for a comparison on the velocity profiles through the VFC with each geometry. Fig. 14 shows the tangential in/out flow through the outlet for each geometry.

This graph primarily depicts two points of interest, firstly, the size of the vortex core, i.e. where air, or for a single-phase case water, is being forced back up through the outlet as a result of pressure differences. Secondly, the speed at which water is moving outwards through the outlet. The circular outlet shows the fastest near wall velocity, followed by the triangle then the square, indicating that more flow is actually moving through the outlet rather than stagnating. The overall fastest core velocity is found with the triangular outlet, it also has the largest core of the three geometries, almost twice as big as that found in a circular outlet. Unexpectedly, the core velocity is higher with the

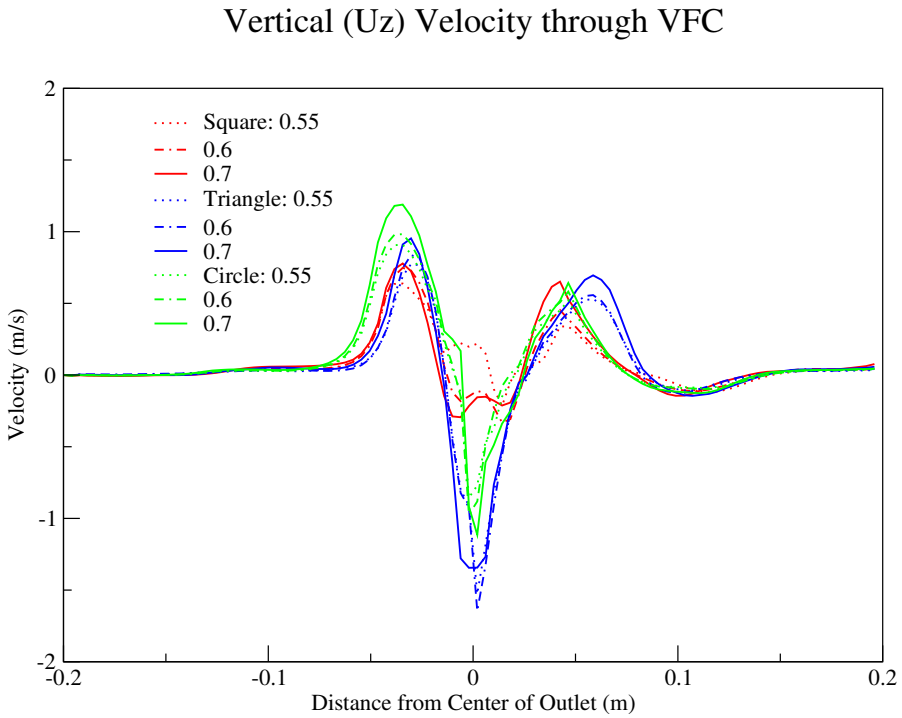

Figure 14. Vertical velocity through the VFC, with positive values being out of it and through the outlet pipe and negative values being backwards into the VFC (backflow).

lower flow velocities in the triangle. This could potentially be as a result of the backflow being restricted to a limiting factor by the fluid characteristics. It is possible that using a single-phase solver has enforced these restrictions, therefore a multi-phase test would be recommended to confirm this, due to the different density and fluid properties of air.

The square outlets perform significantly differently in the core to either of the other two geometries, showing a restricted core with very little backflow, with what could almost be referred to as a double core with the flow velocity slowing as it reaches the very center of the core. It is possible that due to the symmetric nature of the square, slight variations in iterative calculations resulted in the different core sizes and shapes amongst the flow velocities. The core 'deceleration' however, is exhibited by all three velocities, albeit at different locations.

Vertical velocity approaches 0 away from the outlet as expected, a result of the wall boundary conditions on the VFC itself. Taking a slightly higher sample line shows the fluid with a gradual down flow towards the outlet as expected (see Fig. 15).

Not only does Fig. 15 show a more varied velocity through the rest of the VFC as it is not affected by the wall boundary conditions. The velocity magnitude is also depicted in Fig. 16 for flow rates of $5.5Ls^{-1}$ where the cores can be clearly seen for each geometry.

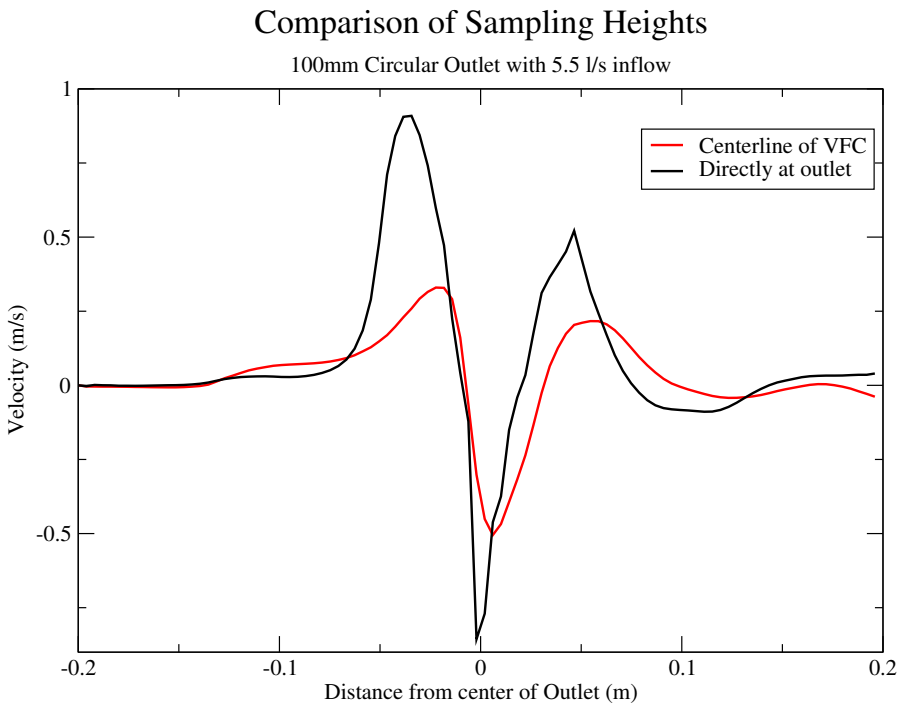

Figure 15. Slightly higher sample line axially across the VFC depicting downwards motion of fluid towards the outlet.

There is a discrepancy when comparing the contour plots with Fig. 14. The vortex cores are off center for both the circular and the square outlets in the contour plots, yet the graph seems to show a core that is centered around the middle of the outlet. This is deceptive as Fig. 16 is a plot of total velocity magnitude which also takes axial velocity into account.

The circular outlet behaves as expected, with a high velocity around the edges of the circle, a high velocity in the very center representing the backflow through the vortex core, and low velocity magnitudes in the core itself.

The triangular outlet shows the unexpected result of higher velocity magnitude in the corners, whereas it was expected that these would be a form of stagnation zone, with the highest velocity being located in the effective vortex. Once again using the sample utility to sample axial components of velocity, the fluid in the corners of the triangle has very little rotation or movement in the axial direction, fluid simply moves through. This defeats the idea of controlling/restricting fluid flow, as the only control is obtained through the vortex, or the incircle, of the triangle.

Theoretically the effective vortex should the largest size of circle able to fit into the

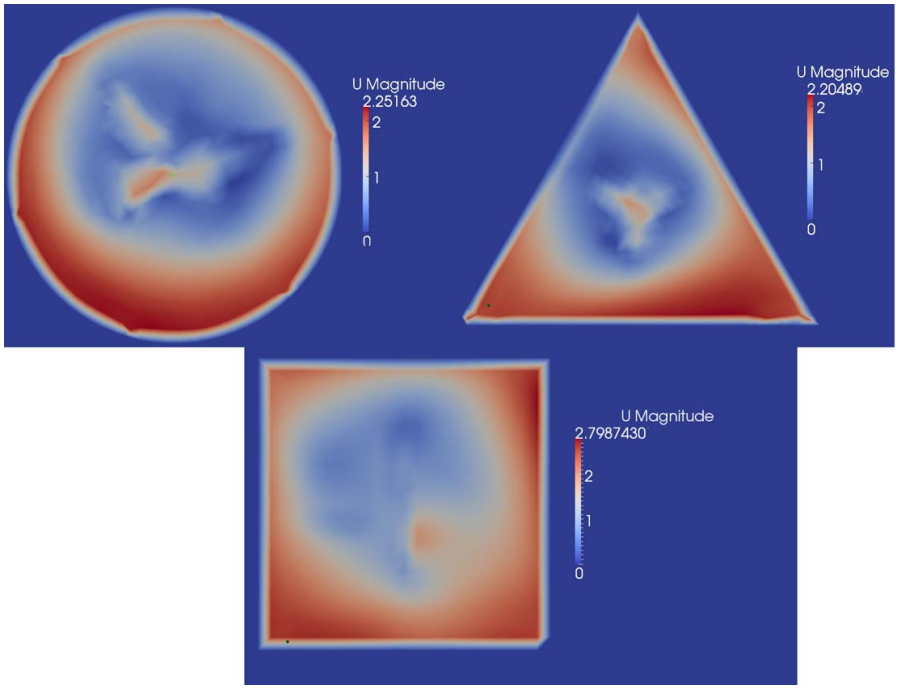

Figure 16. Contour plots of velocity magnitude for all geometries at flow rate of $5.5Ls^{-1}$.

triangle (incircle), which can be obtained by Heron's Formula (Schiefsky, 2007).

$$r_c = \frac{2A}{P} \tag{22}$$

Where r_c is the maximum radius, A is the area of the triangle and P the perimeter. The theoretical value for the triangular outlet used in this project is $38.86mm$. Measuring this from the computational results, one obtains a value of $32mm$, a difference of 17.6%. The difference between these two can be attributed to any number of factors, including iterative errors. Averaging the vortex sizes for all the triangular outlet computations, the difference to the theoretical value decreases further, resulting in a difference of a mere 8%, acceptable when compared to the error differences between experimental and computational data, which are of a similar magnitude.

The square outlet produces results in similar to expectations. In theory the outlet should behave similarly to the triangular outlet, with an effective vortex or incircle. This does seem to be the case, agreeing with the plot in Fig. 14 although there is little to indicate further reasons for the unexpected behaviour of the backflow exhibited.

Contours of the turbulence at each outlet for a flow rate of $5.5Ls^{-1}$ are depicted in Fig. 17. Once again, the actual vortices in these outlets are highly visible, with the

incircle clearly seen in both of the straight sided geometries. The highest turbulence is, as expected, within the incircles, with especially low turbulence in the corners of the straight geometries. This agrees with the velocity findings, showing that flow here does not rotate but merely transitions through the outlet in what could almost be seen as laminar flow.

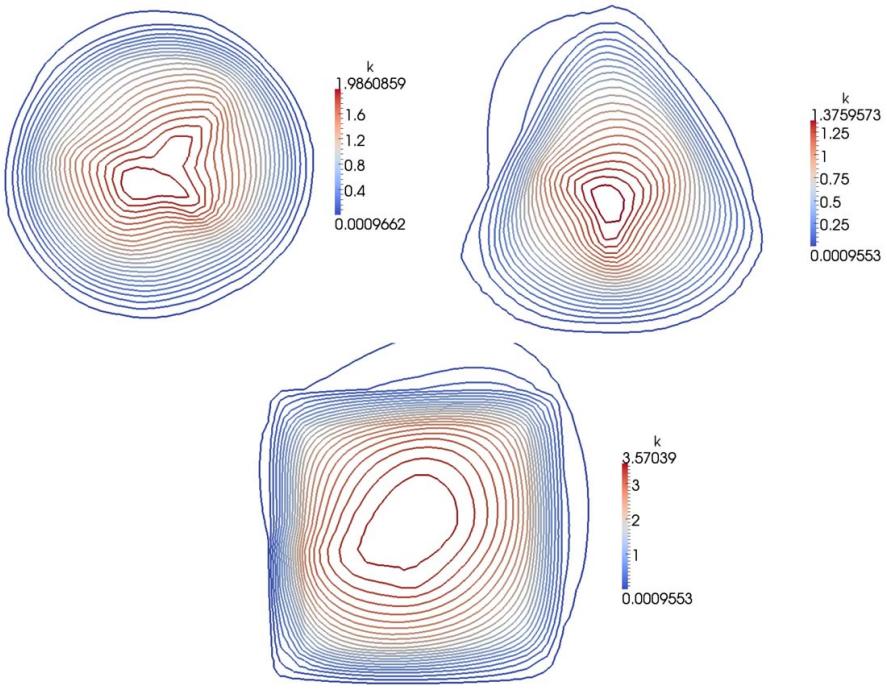

Figure 17. Turbulence contours for the outlet geometries at a flow rate of $5.5Ls^{-1}$.

The circular outlet clearly performs best for the current VFC design at high flow rates. It produces increasingly better head values than either a square or triangular outlet. From the results, it has been seen that the efficiency of a vortex flow control is highly dependent on the size of the effective vortex. Seeing as the area of all outlet geometries was maintained constant throughout, the incircle for the circular outlet was largest, with the triangle having the smallest. This agrees with the findings, which also show that the triangle produces the worst head.

11 Project Planning and Sustainability

As stated in Section 2, the individual task for this research project involves computationally analysing the performance of a vortex flow control at high flow rates, post kickback. Various turbulence models and mathematical approaches will be tested for performance in comparison to data obtained by the experimental section of this group project (Worrall, 2011). Weekly group meetings were held to ensure collaboration between all team members, as well as between the three sections (experimental, urban

drainage and computational). Minutes were taken at every meeting and circulated to all group members, with actions being made for the coming week to ensure adherence to deadlines. A detailed breakdown of the project procedure is detailed below in Fig. 18, as well as being documented in the logbook included with this report submission.

As seen in the chart, multiple process were either delayed or cancelled as the project went on. This was either as a result of time issues or simply changes to the project breakup. Individual tasks for the computational team were initially different to the final sectioning, resulting in modifications being made to the plan.

Originally, one team member was to be responsible for working with the experimental team, modelling the experimental setup, and another two for computationally modelling a real Hydro Brake. These two team members were to design an optimised model and then perform the agreed upon modifications (shape changes) in order to ascertain their effects. This was later changed to a more specific individual group breakdown, with one modelling low flow rates, pre-kickback (see Queguineur (2011)), and another high flow rates, post-kickback. Significant difficulty was encountered in obtaining a working and accurate solution to flow through a hydro brake, resulting in amendments to the original project plan, including the removal of proposed test cases modelling various other aspects that affect flow through a VFC.

All simulations were decomposed to run in parallel on 4 processors in combination with 12Gb of RAM, resulting in a per simulation run time of approximately 48-60 hours. CFD significantly increased the speed at which this project could be completed as well as reducing costs, taking the place of otherwise required experiments and respective equipment. Carbon emissions were also offset as a result of reduced travel time to the testing site at Clevedon, with the only resource used in great quantity being electricity. The unfortunate side effect of running multiple large computations is the resulting processing power and therefore time required for a computer to be kept on. Cases were optimized as much as possible for the scope of this project, so computational/power demand was minimized.

Improvements to project management and group work could have been made in many areas. The quality and quantity of actions made in the weekly meetings should have been increased as should contact between the three sub-groups.

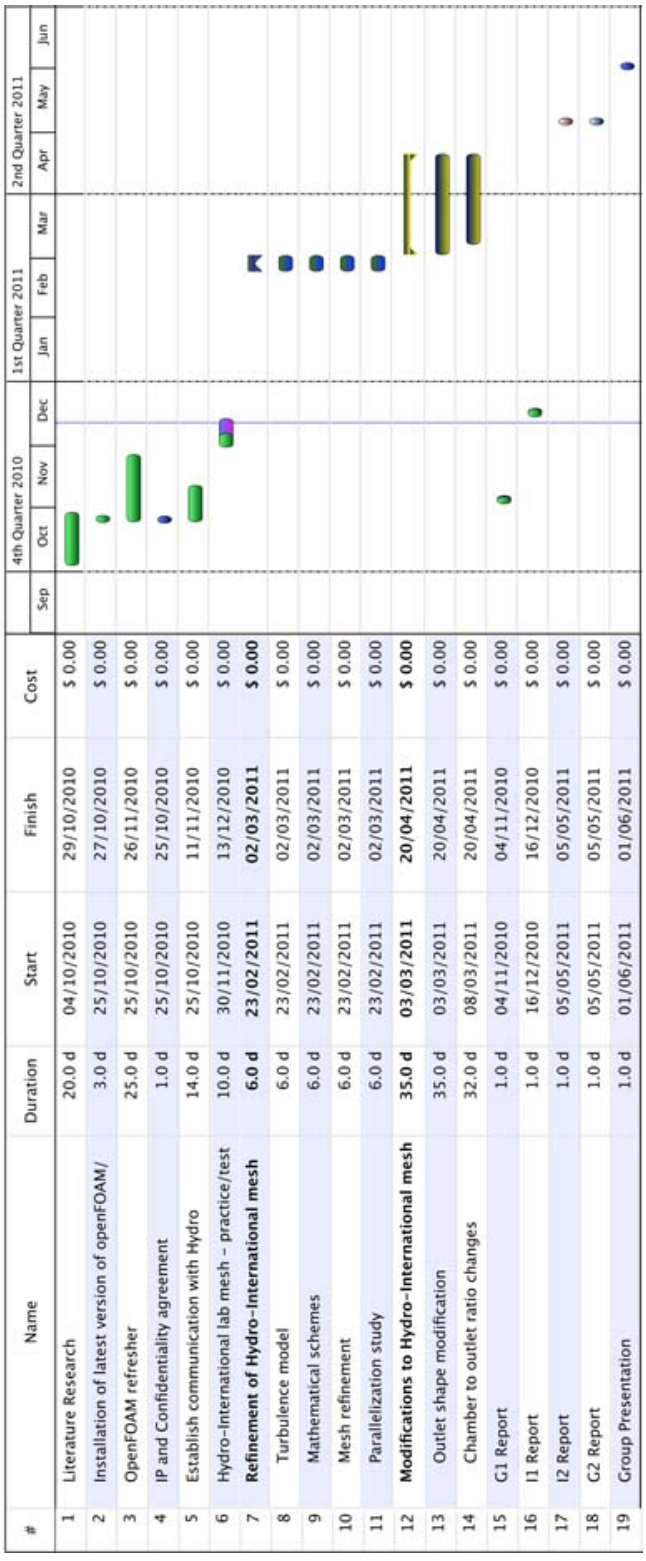

#	Name	Duration	Start	Finish	Cost
1	Literature Research	20.0 d	04/10/2010	29/10/2010	$ 0.00
2	Installation of latest version of openFOAM/	3.0 d	25/10/2010	27/10/2010	$ 0.00
3	OpenFOAM refresher	25.0 d	25/10/2010	26/11/2010	$ 0.00
4	IP and Confidentiality agreement	1.0 d	25/10/2010	25/10/2010	$ 0.00
5	Establish communication with Hydro	14.0 d	25/10/2010	11/11/2010	$ 0.00
6	Hydro-International lab mesh - practice/test	10.0 d	30/11/2010	13/12/2010	$ 0.00
7	**Refinement of Hydro-International mesh**	**6.0 d**	**23/02/2011**	**02/03/2011**	**$ 0.00**
8	Turbulence model	6.0 d	23/02/2011	02/03/2011	$ 0.00
9	Mathematical schemes	6.0 d	23/02/2011	02/03/2011	$ 0.00
10	Mesh refinement	6.0 d	23/02/2011	02/03/2011	$ 0.00
11	Parallelization study	6.0 d	23/02/2011	02/03/2011	$ 0.00
12	**Modifications to Hydro-International mesh**	**35.0 d**	**03/03/2011**	**20/04/2011**	**$ 0.00**
13	Outlet shape modification	35.0 d	03/03/2011	20/04/2011	$ 0.00
14	Chamber to outlet ratio changes	32.0 d	08/03/2011	20/04/2011	$ 0.00
15	G1 Report	1.0 d	04/11/2010	04/11/2010	$ 0.00
16	I1 Report	1.0 d	16/12/2010	16/12/2010	$ 0.00
17	I2 Report	1.0 d	05/05/2011	05/05/2011	$ 0.00
18	G2 Report	1.0 d	05/05/2011	05/05/2011	$ 0.00
19	Group Presentation	1.0 d	01/06/2011	01/06/2011	$ 0.00

Figure 18. The project plan for individual tasks

12 Conclusions

This report focused on modifying the outlet geometry of a Hydro-Brake®flow control, as designed by Hydro-International, in an attempt at increasing its efficiency. More specifically, the performance of the VFC at high flow rates with respect to the aforementioned modifications was tested.

A comprehensive literature review of previous work on vortex diodes was performed, followed by an in depth introduction to diode theory as well as the governing mathematics behind the applicable fluid dynamics. The open source software, OpenFOAM, was introduced in brief, followed by a discussion on actual case configuration, both in OpenFOAM and mesh creation in Gambit.

Two geometry changes, a square and a triangular outlet, were proposed and tested, then compared to a control - a circular outlet as already implemented by Hydro-International. Excellent similarity between computational results and experimental data was found, with an average percentage difference of less than 10%. The triangular outlet was found to create the least head, with the circular outlet creating the most head at the same flow rates. The square outlet also performed well, although less so than the circular outlet. The computations all picked up on the expected vortex core, accurately predicting the locations of expected backflow as well as the velocity profiles throughout the VFC. Discrepancies occurred in the backflow for the square shaped outlet, also growing for all geometries as flow rate increased. Possibilities for error included numerical in the form of iterative error, rounding off and RANS averaging. Other assumptions that were made included the fact that single-phase simulations were sufficient, as were steady-state. It is possible that this is not the case and would require further work. The Reynolds number and respective turbulence variables were calculated based on the VFC inlet, it is possible that taking it from other areas in the VFC, like the outlet, would provide more accurate results.

There is a great quantity of possible further work available on this topic. This report investigated the effect of varying outlet geometry based on the fact that all areas were maintained constant. One could attempt to maintain a constant vortex size rather than constant outlet area, for example, increasing the size of a triangular outlet to make the incircle the same size as the circular outlet. Other work would involve employing other turbulence models, especially the use of LES would be recommended. Alongside this, one could use multi-phase as well as transient solvers to better capture the highly turbulent and developing fluid flow during the initial thousand iterations as found in this investigation.

The efficiency of a VFC, specifically the head, is highly dependent on the maximum vortex size in the outlet. This was smaller for the square and circular outlets as the

maximum vortex was limited to the incircle, which was smaller than the circular outlet. The circular outlet performed the best out of the three geometries for this investigation, producing the most head for each respective flow rate, agreeing with experimental data.

References

Benzi, R. & Frisch, U. (2010). Turbulence. *Scholarpedia*, **5**, 3439.

Derksen, J. (2005). Simulations of confined turbulent vortex flow. *Computers & Fluids*, **34**, 301 – 318.

Derksen, J. & Van den Akker, H.E.A. (2000). Simulation of vortex core precession in a reverse-flow cyclone. *AIChE Journal*, **46**, 1317–1331.

Documentation (2011). OpenFOAM Documentation.

Hydro-International (2010). `http://www.hydro-international.biz`.

Jacobes, B. (1972). The steady-state and transient performance of some large-scale vortex diodes. In *Fifth Cranfield Fluidics Conference, Uppsala*.

Jakirlic, S., Hanjalic, K. & Tropea, C. (2002). Modeling rotating and swirling turbulent flows: A perpetual challenge. *AIAA Journal*, **40**, 0001–1452.

Jarman, D. (2011). *A Study of the Design of Cylindrical Vortex Flow Controls for use in Urban Drainage Systems*. Ph.D. thesis, School of Engineering, Mathematics and Computing, University of Exeter.

Jarman, D., G.Tabor, Butler, D. & Faram, M. (2009). A comparison of rans turbulence models in the prediction of confined turbulent swirling flows in urban drainage flow controls. In *4th OpenFOAM Workshop, Montreal, Canada*.

Jasak, H. (1996). *Error Analysis and Estimation for the Finite Volume Method with Applications to Fluid Flows*. Ph.D. thesis, Department of Mechanical Engineering, University of London, Imperical College.

Jawarneh, A.M. & Vatistas, G.H. (2006). Reynolds stress model in the prediction of confined turbulent swirling flows. *Journal of Fluids Engineering*, **128**, 1377–1382.

Kulkarni, A.A., Ranade, V.V., Rajeev, R. & Koganti, S.B. (2008). Cfd simulation of flow in vortex diodes. *AIChE Journal*, **54**, 1139–1152.

Kulkarni, A.A., Ranade, V.V., Rajeev, R. & Koganti, S. (2009). Pressure drop across vortex diodes: Experiments and design guidelines. *Chemical Engineering Science*, **64**, 1285 – 1292.

Launder, B.E. & Sharma, B.I. (1974). Application of the energy-dissipation model of turbulence to the calculation of flow near a spinning disc. *Letters in Heat and Mass Transfer*, **1**, 131–138.

Launder, B.E., Reece, G.J. & Rodi, W. (1975). Progress in the development of a reynolds-stress turbulent closure. *Journal of Fluid Mechanics*, **68**, 537–566.

Mathieu, J. & Scott, J. (2000). *An Introduction to Turbulent Flow*. Cambridge University Press.

McLachlan, R.I. (1998). Spatial discretization of partial differential equations with integrals. *ArXiv Mathematics e-prints*.

Peric, M. (1985). *A Finite Volume method for the Prediction of Three-Dimensional Fluid Flow in Complex Ducts*. Ph.D. thesis, Imperial College, University of London.

Priestman, G. & Tippetts, J. (1984). Development and potential of power fluidics for process flow control. *Chem. Eng. Res. Design*, **62a**.

Priestman, G.H. (1987). A study of vortex throttles part 1: experimental. *ARCHIVE: Proceedings of the Institution of Mechanical Engineers, Part C: Mechanical Engineering Science 1983-1988 (vols 197-202)*, **201**, 331–336.

Queguineur, G. (2011). *Computational Investigation of Multi-Phase Vortex Flow Control Operating at Low Flow Rates*. Master's thesis, School of Engineering, Mathematics and Computing, University of Exeter.

Rogers, G.F.C. & Mayhew, Y.R. (1995). Thermodynamic and Transport Properties of Fluids. Booklet.

Schiefsky, M.J. (2007). *Theory and practice in Heron's Mechanics*. Springer Verlag, New York.

Smagorinsky, J. (1963). General circulation experiments with the primitive equations, i. the basic experiment. *Monthly Weather Review*, **91**, 99–164.

Speziale, C., Sarkar, S. & Gatski, T. (1991). Modeling the pressure-strain correlation of turbulence: an invariant dynamical systems approach. *Journal of Fluid Mechanics*, **227**, 245–272.

Stairmand, J. (1990). Flow patterns in vortex chambers for nuclear duties. *Nuclear Energy*, **29**.

Tabor, G.R. & Baba-Ahmadi, M.H. (2008). Inlet conditions for large eddy simulation of gas-turbine swirl injectors. *AIAA Journal*, **46**, 1782–1790.

Toro, E.F. (1999). *Riemann Solvers and Numerical Methods for Fluid Dynamics*. Springer-Verlag.

Uddin, N. (2008). *Turbulence Modeling of Complex Flows in CFD*. Ph.D. thesis, Faculty of Aerospace Engineering and Geodesy, Universitaet Stuttgart.

Wilcox, D. (1988). Re-assessment of the scale-determining equation for advanced turbulence models. *AIAA Journal*, **26**, 1414–1421.

Wormley, D. & Richardson, H. (1970). A design basis for vortex type fluid amplifier operating in the incompressible flow regime. *Transactions of ASME: Journal of Basic Engineering*, **91D**.

Worrall, E. (2011). *Experimental Testing and Analysis of Modified Vortex Flow Controls at Hydro-International Plc.*. Master's thesis, School of Engineering, Mathematics and Computing, University of Exeter.

Yin, J., Jiao, L. & Wang, L. (2010). Large eddy simulation of unsteady flow in vortex diode. *Nuclear Engineering and Design*, **240**, 970 – 974.

Zobel, R. (1930). Experiments on a hydraulic reversing throat. *Mitt. Hydraul. Munich*, **8**, 1–47.

A Flow Control Drawings

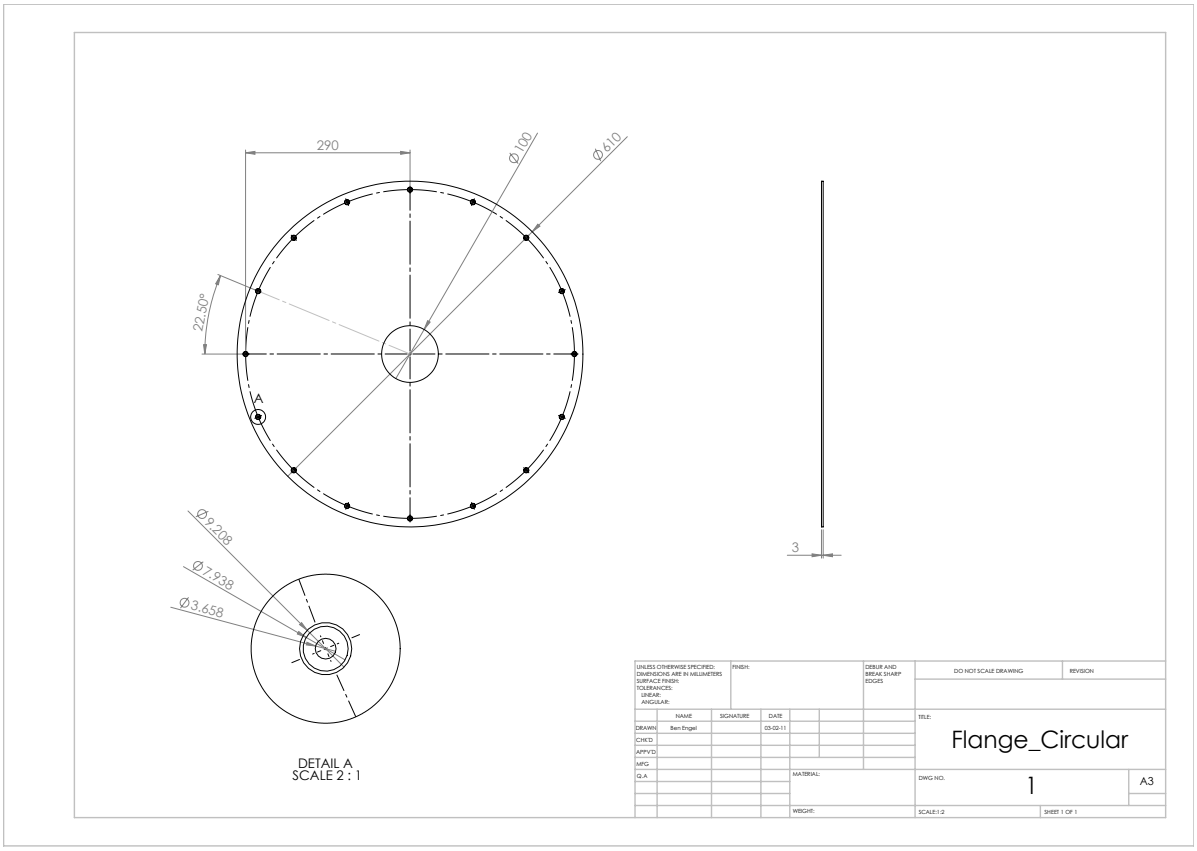

Figure 19. Circular outlet

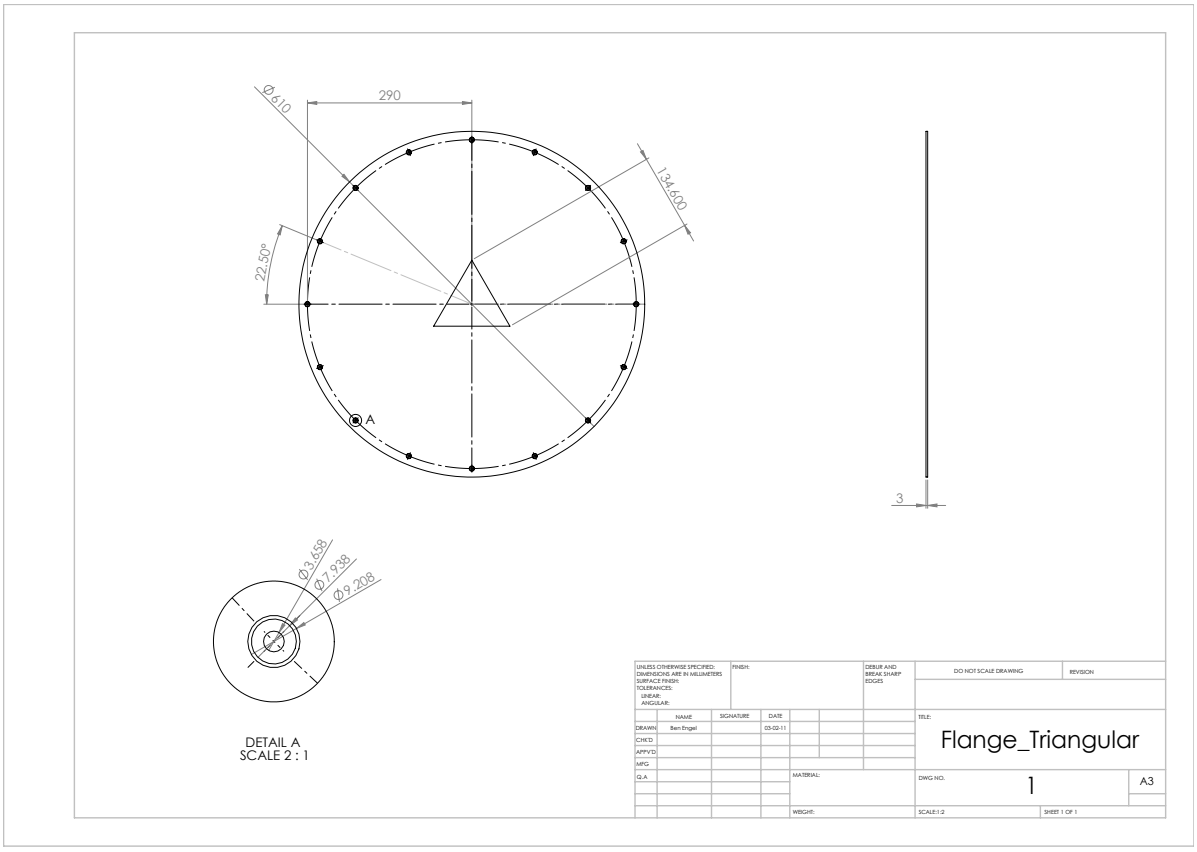

Figure 20. Triangular outlet

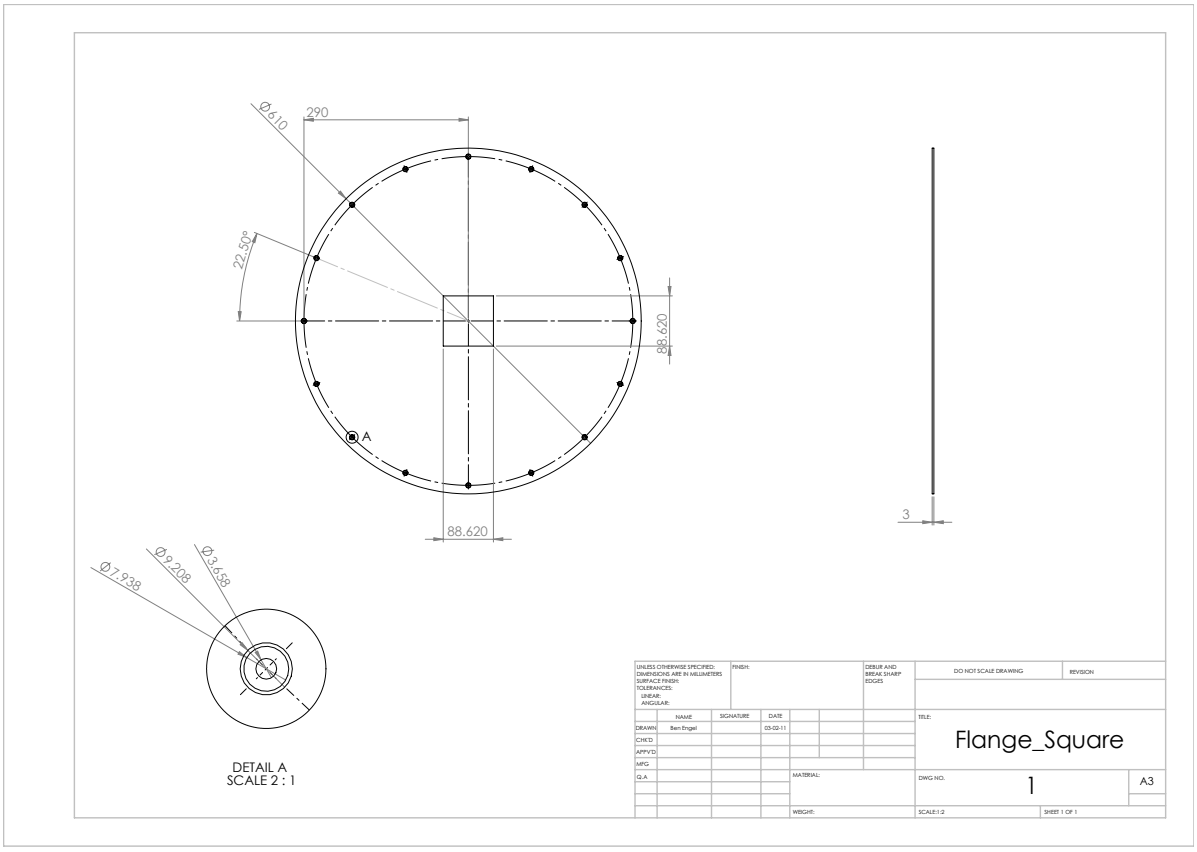

Figure 21. Square outlet